Accurate and Efficient Algorithm for Computing Structure Functions from the Spatial Distribution of Thermal Properties in Electronic Devices

Lorenzo Codecasa, *Member, IEEE*, Vincenzo d'Alessandro, Antonio Pio Catalano, Ciro Scognamillo, Dario D'Amore, *Member, IEEE*, and Klaus Aufinger, *Member, IEEE*

***Abstract*—An accurate and efficient algorithm is presented, which allows deriving the structure function of a discretized 3-D heat conduction problem. In this approach, the partial thermal conductances and capacitances in the structure function are computed in terms of weighted spatial averages of thermal resistivity and volumetric heat capacity. As a result, the exact influence of all materials and geometric details on each part of the structure function is determined. The approach is validated on a state-of-the-art SiGe HBT for high-frequency applications.**

***Index Terms*—Heterojunction bipolar transistor (HBT), multi-directional heat flow, self-heating (SH), silicon germanium (SiGe), structure function, transmission line.**

I. INTRODUCTION

THE *structure functions*–introduced by Protonotarios and Wing in 1967 [1]–were identified as a useful means for the thermal characterization of electronic devices by Székely and Van Bien [2], and are today largely used in the semiconductor industry for failure analysis and to improve the thermal models of the products. Originally, the structure functions have been considered for domains where the heat flow is, at least approximately, *one-directional* [2]. A one-directional heat flow corresponds to a one-dimensional (1-D) heat conduction problem in which the power is injected at one boundary and the temperature rise is measured at the same boundary, and is equivalent to a short-circuited *RC* transmission line. From the electric circuit theory, it is well known that the structure function of such a transmission line can be completely recovered from its port response, either in the time or frequency domain [1]. As a result, interesting information on the spatial distribution of thermal properties of a one-directional heat conduction problem can be gained.

A two-step algorithm was developed by Székely for reconstructing a structure function from the experimental or numerically-simulated thermal response [2], [3]: first, such a response is described with a lumped *RC* one-port network in the Foster's I canonical form, derived by inverse numerical deconvolution [4]; second, an approximation of the structure function is obtained by a simple transformation of the Foster's network into the ladder-shaped Cauer's I canonical form, performed with a long-division procedure.

However, the Székely's algorithm presented in [2], [3] suffers from a limited accuracy and is very sensitive to the input data [5]. Conveniently, such drawbacks have been mitigated in an improved, yet non-documented, algorithm variant commercially available in the Siemens-Mentor T3Ster and FloTHERM software packages. This variant has been *heuristically* used also for generic *multi-directional* (i.e., non-one-directional) heat flow problems by Székely and his coworkers [6], [7]. The applicability of the approach to a multi-directional heat propagation was confirmed by Codecasa [8], who *rigorously* proved that any one-port passive dynamic thermal network modeling a three-dimensional (3-D) heat conduction problem is still characterized by a structure function.

Unfortunately, in the multi-directional case, the structure function extracted with the improved Székely's algorithm cannot be related to the spatial distribution of thermal properties in the examined domain; consequently, no useful information can be gained from it [9].

In [10], we presented an accurate and efficient algorithm that can be exploited to derive a structure function from the discretized equation governing the 3-D heat conduction problem in any electronic device. Unlike the common approximate approach based on the solution of the discretized thermal model, the proposed methodology *directly* (i.e., without computing the thermal response) and *exactly* derives the *RC* ladder network defining the structure function of the device; this is done by means of a Lanczos-like tridiagonalization algorithm applied to the pair of mass and stiffness matrices used for discretizing the heat conduction in the domain. By using such an approach, each resistance and capacitance of the *RC* ladder network is computed in terms of weighted spatial averages of thermal resistivity and volumetric heat capacity over a sub-region of the device. For increasing values of the cumulative capacitances and resistances, that sub-region gradually expands from the heat source to the entire spatial domain. In this way, for the first time in literature, the *exact* correspondence between the structure function of the device and the spatial distribution of its thermal properties can be determined in 3-D heat conduction problems of practical interest. This achievement is consistent with–and completes–the

L. Codecasa and D. D'Amore are with the Department of Electronics, Information, and Bioengineering, Politecnico di Milano, 20133 Milan, Italy (e-mail: lorenzo.codecasa@polimi.it).

V. d'Alessandro, A. P. Catalano, and C. Scognamillo are with the Department of Electrical Engineering and Information Technology, University Federico II, via Claudio 21, 80125 Naples, Italy (e-mail: vindales@unina.it). (*Corresponding author: Vincenzo d'Alessandro*)

K. Aufinger is with Infineon Technologies AG, 85579 Neubiberg, Germany (e-mail: Klaus.Aufinger@infineon.com).

theoretical result proved by Codecasa [11], who found a strong relation between the structure function and the spatial distribution of thermal properties in a generic multi-directional case by means of wave-fronts and rays of a wave propagation problem associated to the heat conduction problem.

The proposed algorithm can be practically exploited by applying the following procedure, which generalizes what is commonly done with structure functions of one-directional heat flow problems. Let us assume that the 3-D thermal model of a device has been built and that its structure function has been extracted by the proposed algorithm. Let us also assume that the structure function of the real device has been derived from the thermal response by using other algorithms (e.g., the commercial variant of the Székely algorithm or our more robust version of it presented in Section V.A). The inspection of (possible) discrepancies between these structure functions, supported by the correspondence between our structure function and the spatial distribution of thermal properties, could help (i) calibrate the thermal properties of the model, and/or (ii) localize defects and other problems due to technological tolerances in the real device. The feasibility of our approach for this application is demonstrated in Section V.B by comparing the structure functions extracted by our algorithm from the thermal models of a reference device and a variant of it where a technological parameter was modified *ad hoc*. As the relevant portion of the structure function is usually determined in a short time (a few minutes), it is expected that the proposed approach may offer a valuable aid for design engineers.

Here we extend [10] in a two-fold way: (i) by providing a detailed explanation of the algorithm, and (ii) by validating the methodology on a state-of-the-art device under test (DUT) with a geometrically-complex structure and a markedly 3-D heat flow. More specifically, the DUT is a single-emitter silicon-germanium (SiGe) heterojunction bipolar transistor (HBT) with excellent frequency performance, yet suffering from a high self-heating (SH) thermal resistance.

The remainder of this paper is arranged as follows. In Section II, the concept of structure function is recalled for one-directional and multi-directional heat flows. Section III introduces the novel algorithm for extracting the structure function. In Section IV, the details of the DUT are given. In Section V, results are presented and discussed. The conclusion is drawn in Section VI.

II. STRUCTURE FUNCTIONS

A. One-directional Heat Flow

Let us consider a heat conduction problem in a cylinder Ω of length L and cross-section area A, in which the longitudinal coordinate x varies from 0 to L. Let us assume that (i) the thermal properties are uniform at each normal cross-section of Ω, (ii) the heat flux across the boundary surface $x=0$ is uniform, (iii) the temperature rise at the boundary surface $x=L$ is zero, and (iv) the heat flux across the lateral boundary surface is zero. This specific thermal problem is referred to as one-directional heat flow [2] and is governed by the following equations:

$$\frac{\partial q}{\partial x}(x,t)+c(x)\frac{\partial \vartheta}{\partial t}(x,t)=0 \tag{1}$$

$$q(x,t)=-k(x)\frac{\partial \vartheta}{\partial x}(x,t) \tag{2}$$

in which $\vartheta(x,t)$ is the temperature rise over ambient, $q(x,t)$ is the heat flux component along x, $c(x)$ is the volumetric heat capacity, and $k(x)$ is the thermal conductivity. The boundary conditions are $q(0,t)=P(t)/A$ and $\vartheta(L,t)=0$, $P(t)$ being the total power injected at the boundary $x=0$. The initial condition is assumed to be zero. By introducing the *cumulative capacitance* C and *cumulative resistance* R along the heat flow path

$$C(x)=\int_0^x Ac(\xi)d\xi \tag{3}$$

$$R(x)=\int_0^x \frac{1}{Ak(\xi)}d\xi \tag{4}$$

(1), (2) can be rewritten in the equivalent form

$$\frac{\partial Q}{\partial R}(x(R),t)+\frac{d}{dR}S(R)\frac{\partial \vartheta}{\partial t}(x(R),t)=0 \tag{5}$$

$$Q(x(R),t)=-\frac{\partial \vartheta}{\partial R}(x(R),t) \tag{6}$$

in which $Q(x(R),t)=Aq(x(R),t)$, and $C=S(R)$ is the *(cumulative) structure function*, obtained by eliminating the x variable among (3), (4). These equations define a passive RC transmission line short-circuited at the output port, having as input port variables the power $P(t)$ and the temperature rise $\Delta T(t)=\vartheta(0,t)$. The $C=S(R)$ function relates the cumulative capacitance C to the cumulative resistance R along the line [1]. From (3), (4), it straightforwardly ensues

$$\frac{d}{dR}S(R)=A^2c(x)k(x) \tag{7}$$

which associates the (differential) structure function $\mathrm{d}C/\mathrm{d}R$ at R to the thermal properties $c(x)$, $k(x)$ at x related to R by (4). Eq. (7) establishes the relation between the structure function and the spatial distribution of thermal properties in one-directional heat flow problems.

The structure functions can be uniquely determined from the input-port thermal response of the short-circuited RC transmission line $z(t)$ relating the injected power $P(t)$ to the temperature rise $\Delta T(t)$ by $\Delta T(t)=z(t)*P(t)$, $*$ being the convolution operator. A two-step Székely's algorithm [2], [3] is usually adopted for reconstructing the structure function from the response $z(t)$: first, a lumped RC one-port network in the Foster's I canonical form describing the thermal response is derived by inverse numerical deconvolution; second, an approximation of the structure function is obtained by a long-division transformation of this network into the ladder-shaped Cauer's I form. Fig. 1 shows the RC transmission line and the Cauer's network, along with the corresponding structure functions. A commercial, yet poorly-documented, variant of this algorithm is broadly exploited to characterize the heat propagation in electronic devices from their experimental thermal response [6], [7]. However, in generic multi-directional cases, the interpretation of structure function previously recalled no longer holds, which prevents from deriving detailed information on the thermal properties of the domain [9].

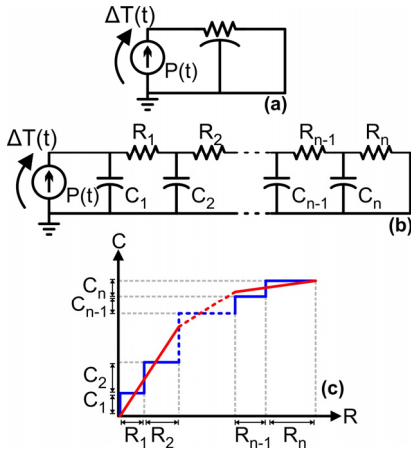

Fig. 1. (a) *RC* transmission line and (c) corresponding structure function (red line); (b) Cauer's I ladder network approximating the transmission line and (c) associated structure function (blue line).

B. Multi-Directional Heat Flow

Let us consider a multi-directional heat conduction problem in a bounded region Ω. The relation between the power density $g(\mathbf{r},t)$, the temperature rise $\vartheta(\mathbf{r},t)$, and the heat flux $\mathbf{q}(\mathbf{r},t)$ at position $\mathbf{r}$ and time instant t is governed by

$$\nabla\cdot\mathbf{q}(\mathbf{r},t)+c(\mathbf{r})\frac{\partial\vartheta}{\partial t}(\mathbf{r},t)=g(\mathbf{r},t) \tag{8}$$

$$\mathbf{q}(\mathbf{r},t)=-k(\mathbf{r})\nabla\vartheta(\mathbf{r},t) \tag{9}$$

in which $c(\mathbf{r})$ is the volumetric heat capacity and $k(\mathbf{r})$ is the thermal conductivity, considered as scalar for the sake of simplicity. Conditions on the boundary $\partial\Omega$, assumed of Robin's type, are

$$\mathbf{q}(\mathbf{r},t)\cdot\mathbf{v}(\mathbf{r})=h(\mathbf{r})\vartheta(\mathbf{r},t) \tag{10}$$

in which $h(\mathbf{r})$ is the heat transfer coefficient and $\mathbf{v}(\mathbf{r})$ is the unit vector outward normal to $\partial\Omega$. Initial conditions are assumed to be zero.

A one-port passive dynamic thermal model can be defined consistently with [8] by introducing the power $P(t)$ and the temperature rise $\Delta T(t)$ measured at its port as follows. The power $P(t)$ determines the power density as

$$g(\mathbf{r},t)=g(\mathbf{r})P(t) \tag{11}$$

in which $g(\mathbf{r})$ is a shape function of support Σ. The port temperature rise is the weighted average

$$\Delta T(t)=\int_{\Omega} g(\mathbf{r})\vartheta(\mathbf{r},t)\,d\mathbf{r} \tag{12}$$

Like in the one-directional case, the port response of this one-port passive dynamic thermal model is described by the thermal response $z(t)$ such that $\Delta T(t)=z(t)*P(t)$. Moreover, as demonstrated by Codecasa [8], this one-port passive dynamic thermal model can be exactly modeled by a passive *RC* transmission line characterized by a structure function $C=S(R)$, like in the one-directional case. Also, such a structure function can again be uniquely reconstructed from the thermal response.

A strong relation between the structure function $C=S(R)$ and the spatial distribution of thermal properties has been established by Codecasa [11] by considering the following wave propagation problem in Ω, companion to the previous heat conduction problem

$$\nabla\cdot\mathbf{j}(\mathbf{r},t)+c(\mathbf{r})\frac{\partial\varphi}{\partial t}(\mathbf{r},t)=g(\mathbf{r},t) \tag{13}$$

$$\frac{\partial\mathbf{j}}{\partial t}(\mathbf{r},t)=-k(\mathbf{r})\nabla\varphi(\mathbf{r},t) \tag{14}$$

with boundary conditions in $\partial\Omega$

$$\frac{\partial\mathbf{j}}{\partial t}(\mathbf{r},t)\mathbf{v}(\mathbf{r})=h(\mathbf{r})\varphi(\mathbf{r},t) \tag{15}$$

and homogeneous initial conditions. By construction the spatial distributions of $c(\mathbf{r})$, $k(\mathbf{r})$, and $h(\mathbf{r})$ are common to the heat conduction and the companion wave propagation problems.

A one-port *lossless* dynamic model can be introduced by defining the current $I(t)$ and voltage $V(t)$ measured at its port. The current $I(t)$ determines $g(\mathbf{r},t)$ as

$$g(\mathbf{r},t)=g(\mathbf{r})I(t) \tag{16}$$

The voltage $V(t)$ is the weighted mean

$$V(t)=\int_{\Omega} g(\mathbf{r})\varphi(\mathbf{r},t)\,d\mathbf{r} \tag{17}$$

As proved in [11], this one-port lossless dynamic model can be described by a short-circuited *LC* transmission line characterized by the same structure function $C=S(L)$ modeling the passive *RC* transmission line, where L is the cumulative inductance and C is the cumulative capacitance along the *LC* transmission line.

Considering such a companion wave propagation problem, let $\varphi(\mathbf{r},t)$, $\mathbf{j}(\mathbf{r},t)$ be the solution of the wave propagation problem due to a unit impulse $I(t)$. Let $\omega_c(\tau)$ be the sub-region of Ω in each point of which $\varphi(\mathbf{r},t)\neq 0$ at some $t\leq\tau$, and let $\partial\omega_c(\tau)$ be its boundary. Similarly, let $\omega_k(\tau)$ be the sub-region of Ω, in each point of which $\mathbf{j}(\mathbf{r},t)\neq\mathbf{0}$ at some $t\leq\tau$, and let $\partial\omega_k(\tau)$ be its boundary.

The $\omega_c(\tau)$ and $\omega_k(\tau)$ regions can be characterized as follows. The $\omega_c(0)$ region is the support of $\varphi(\mathbf{r},0)=g(\mathbf{r})/c(\mathbf{r})$, that is, Σ. Similarly, the $\omega_k(0)$ region is the support of $\mathbf{j}(\mathbf{r},0)$, which is a sub-region of Σ. The $\partial\omega_c(t)$ and $\partial\omega_k(t)$ surfaces are the *wave-fronts* of $\varphi(\mathbf{r},t)$ and $\mathbf{j}(\mathbf{r},t)$, respectively, which propagate at finite velocity, at each $\mathbf{r}$ given by $\sqrt{k(\mathbf{r})/c(\mathbf{r})}$.

In force of this link between a heat conduction problem and its companion wave propagation problem, the following result holds [11]: *for each R, the restriction of the structure function $C=S(R)$ to the range $[0, R]$ is affected by all and only the values of $c(\mathbf{r})$ in $\omega_c(\tau)$ and of $k(\mathbf{r})$, $h(\mathbf{r})$ in $\omega_k(\tau)$, being*

$$\tau=\int_0^R\sqrt{\frac{dS}{dR}}dR \tag{18}$$

The novel algorithm introduced in Section III will allow further extending this relation between the structure function and the spatial distribution of thermal properties.

III. NOVEL ALGORITHM FOR COMPUTING STRUCTURE FUNCTIONS

The heat conduction problem, discretized either (i) by the finite-volume method (FVM) over a hexahedral grid (composed by rectangular parallelepipeds, often denoted as

bricks), or (ii) by the finite-element method (FEM) e.g., over a hexahedral or tetrahedral grid, can be put in the form

$$\mathbf{M}\frac{\partial \boldsymbol{\vartheta}}{\partial t}(t)-\mathbf{D}^T\mathbf{q}(t)=\mathbf{g}(t) \tag{19}$$

$$\mathbf{q}(t)=-\boldsymbol{\Lambda}\mathbf{D}\boldsymbol{\vartheta}(t) \tag{20}$$

in which $\boldsymbol{\vartheta}(t)$ is an N-column vector with the degrees of freedom (DoFs) of the temperature rise, $\mathbf{q}(t)$ is an E-column vector with the DoFs of the heat flux, $\mathbf{D}$ is the $E\times N$ rectangular matrix discretizing the gradient operator, $\mathbf{M}$ is the N-order mass matrix, and $\boldsymbol{\Lambda}$ is an E-order symmetric positive definite matrix discretizing the thermal conductivity constitutive relation. By eliminating the $\mathbf{q}(t)$ variables in (19), (20), it is obtained that

$$\mathbf{M}\frac{\partial \boldsymbol{\vartheta}}{\partial t}(t)+\mathbf{K}\boldsymbol{\vartheta}(t)=\mathbf{g}(t) \tag{21}$$

in which $\mathbf{K}=\mathbf{D}^T\boldsymbol{\Lambda}\mathbf{D}$ is the N-order stiffness matrix. The one-port passive dynamic thermal model is defined introducing the relations

$$\mathbf{g}(t)=\mathbf{g}P(t) \tag{22}$$

$$\Delta T(t)=\mathbf{g}^T\boldsymbol{\vartheta}(t) \tag{23}$$

determining its port variables $P(t)$ e $\Delta T(t)$.

The Cauer's I canonical form of this one-port dynamic thermal model is governed by

$$\mathbf{C}\frac{d\mathbf{x}}{dt}(t)+\mathbf{G}\mathbf{x}(t)=\mathbf{e}_1P(t) \tag{24}$$

$$T(t)=\mathbf{e}_1^T\mathbf{x} \tag{25}$$

in which $\mathbf{x}(t)$ is the N-column vector of the electrical potentials at the N nodes, and $\mathbf{e}_1$ is an N-column vector with all elements equal to 0 but the first element, which is equal to 1.

The N-order diagonal matrix $\mathbf{C}$ and the N-order tridiagonal matrix $\mathbf{G}$ take the form

$$\mathbf{C}=\begin{bmatrix} C_1 & 0 & \cdots & 0 \\ 0 & C_2 & \ddots & \vdots \\ \vdots & \ddots & \ddots & 0 \\ 0 & \cdots & 0 & C_N \end{bmatrix}$$

$$\mathbf{G}=\begin{bmatrix} G_1 & -G_1 & 0 & \cdots & 0 \\ -G_1 & G_1+G_2 & \ddots & & \vdots \\ 0 & \ddots & \ddots & \ddots & 0 \\ \vdots & & \ddots & \ddots & -G_{N-1} \\ 0 & \cdots & 0 & -G_{N-1} & G_{N-1}+G_N \end{bmatrix}$$

where C_k is the capacitance of the capacitor connecting the k-th node to ground, with k=1, ..., N, and G_k is the conductance of the resistor connecting the k-th node to the k+1-th, with k=1, ..., N-1.

Eqs. (21)-(23) can be transformed into (24), (25) governing the Cauer's I canonical form by the following approach. Let $\mathbf{V}$ be a nonsingular N-order matrix such that

$$\mathbf{V}^T\mathbf{M}\mathbf{V}=\mathbf{I} \tag{26}$$

$$\mathbf{V}^T\mathbf{K}\mathbf{V}=\mathbf{T} \tag{27}$$

where $\mathbf{I}$ is the identity matrix, and $\mathbf{T}$ is a symmetric tridiagonal matrix

$$\mathbf{T}=\begin{bmatrix} \alpha_1 & -\beta_1 & 0 & \cdots & 0 \\ -\beta_1 & \alpha_2 & \ddots & & \vdots \\ 0 & \ddots & \ddots & \ddots & 0 \\ \vdots & & \ddots & \ddots & -\beta_{N-1} \\ 0 & \cdots & 0 & -\beta_{N-1} & \alpha_N \end{bmatrix}$$

and such that

$$\mathbf{V}^T\mathbf{g}=\beta_0\mathbf{e}_1 \tag{28}$$

Then, by using the transformation of variables

$$\boldsymbol{\vartheta}(t)=\mathbf{V}\boldsymbol{\xi}(t) \tag{29}$$

(21)-(23) can be written in the equivalent form

$$\frac{d\boldsymbol{\xi}}{dt}(t)+\mathbf{T}\boldsymbol{\xi}(t)=\beta_0\mathbf{e}_1P(t) \tag{30}$$

$$\Delta T(t)=\beta_0\mathbf{e}_1^T\boldsymbol{\xi}(t) \tag{31}$$

The tridiagonal Eqs. (30), (31) can in turn be straightforwardly transformed into the Cauer's I canonical form given by (24), (25) by the simple rescaling of variables

$$\boldsymbol{\xi}(t)=\mathbf{C}^{1/2}\mathbf{x}(t) \tag{32}$$

Thus it ensues that $C_1=1/\beta_0^2$, and that

$$G_k=\alpha_kC_k-G_{k-1} \quad \text{for } k=1, ..., N \tag{33}$$

$$C_{k+1}=\frac{1}{\beta_k^2}\frac{G_k^2}{C_k} \quad \text{for } k=1, ..., N-1 \tag{34}$$

assuming G_0=0. Hence, each value of the conductance G_k and capacitance C_{k+1} in the Cauer's I canonical form can be determined by the α_k and β_k coefficients in the tridiagonal equations in addition to the values of previous conductances G_{k-1} and capacitances C_k, respectively.

The α_k and β_k coefficients can be evaluated by a tridiagonalization algorithm [12] suited to determine the $\mathbf{V}$ matrix satisfying (26)-(28). The algorithm adopted here, derived adapting the Lanczos' algorithm, is reported below.

Adapted Lanczos' algorithm

$\boldsymbol{\nu}_0 := \mathbf{0}$
Solve $\mathbf{M}\boldsymbol{\varphi}_0 = \mathbf{g}$ for $\boldsymbol{\varphi}_0$
$\beta_0^2 := \boldsymbol{\varphi}_0^T\mathbf{M}\boldsymbol{\varphi}_0$
$k := 0$
while $\beta_k \neq 0$ **do**
  $k := k+1$
  $\boldsymbol{\nu}_k := \boldsymbol{\varphi}_{k-1}/\beta_{k-1}$
  $\mathbf{j}_k := -\boldsymbol{\Lambda}\mathbf{D}\boldsymbol{\nu}_k$
  $\alpha_k := \mathbf{j}_k^T\boldsymbol{\Lambda}^{-1}\mathbf{j}_k$
1 Solve $\mathbf{M}\boldsymbol{\varphi}_k = -\mathbf{D}^T\mathbf{j}_k + \mathbf{M}(\alpha_k\boldsymbol{\nu}_k - \beta_{k-1}\boldsymbol{\nu}_{k-1})$ for $\boldsymbol{\varphi}_k$
  $\beta_k^2 := \boldsymbol{\varphi}_k^T\mathbf{M}\boldsymbol{\varphi}_k$

This algorithm successively computes the columns $\boldsymbol{\nu}_k$ of the transformation matrix $\mathbf{V}$, with k=1, ..., N.

Using the proposed algorithm, the conductances G_k and capacitances C_k defining the structure function of the discretized heat conduction problem can be efficiently

determined for the following reasons: (i) no computationally expensive transient simulations of the heat conduction problem have to be performed; (ii) each iteration is fast since it only requires to solve the matrix equation at line 1, which can be very quickly done: when the FVM is adopted for discretizing the heat conduction problem, no matrix equation has indeed to be solved since the mass matrix $\mathbf{M}$ is diagonal; when the FEM is used, the conjugate gradient method can be invoked to solve the equation with a few iterations only; (iii) the number of steps of the algorithm needed to reconstruct the significant part of the structure function (where the wave-front has not propagated yet very far away from the source) is not N, but is in the order of the number of the discretization points in each direction, that is, $N^{1/3}$; (iv) the proposed Lanczos-like tridiagonalization algorithm, when exploited for the extraction of a structure function from a discretized heat conduction model, can be applied as is, without the necessity of improving its robustness through selective orthonormalization [12], which would add computational burden.

At each step of the algorithm, the α_k coefficient determining the G_k partial conductance of the structure function (blue line in Fig. 1) is expressed as the spatial average of the inverse of thermal conductivity weighted by the field $\mathbf{j}_k(\mathbf{r})$ having $\mathbf{j}_k$ as DoF,

$$\alpha_k = \mathbf{j}_k^T \mathbf{\Lambda}^{-1} \mathbf{j}_k = \int_\Omega \frac{\mathbf{j}_k^2(\mathbf{r})}{k(\mathbf{r})} d\mathbf{r} \tag{35}$$

Similarly, the β_k coefficient determining the C_{k+1} partial capacitance of the structure function is expressed as the spatial average of the volumetric heat capacity weighted by the field $\varphi_k(\mathbf{r})$, having φ_k as DoF

$$\beta_k^2 = \varphi_k^T \mathbf{M} \varphi_k = \int_\Omega c(\mathbf{r}) \varphi_k^2(\mathbf{r}) d\mathbf{r} \tag{36}$$

As a result, the exact dependence of the structure function on thermal properties is provided in terms of averages of thermal properties distributions.

IV. DEVICE UNDER TEST

The SiGe HBT technology is currently used in a large variety of commercial and research applications in the mm- and even sub-mm-wave frequency spectrum, like automotive radars, high-bandwidth communication, material science, medical equipment, and optical transmission [13]–[16]. Unfortunately, boosting the frequency performance of such transistors unavoidably leads to significant SH induced by (i) the higher current/power densities, and (ii) the higher thermal resistances R_{TH} due to the lateral scaling of the intrinsic transistor and the adoption of shallow/deep trenches filled with low thermal conductivity materials. In particular, the R_{TH}s have been pushed beyond 10^3 K/W [17]–[20] and can even exceed 10^4 K/W for small devices with superior RF performance [21]–[23].

Here the analysis is performed on a single-emitter SiGe:C NPN HBT with one base and one collector contact (BEC configuration) manufactured by Infineon Technologies AG within the framework of the DOTFIVE project. More specifically, the DUT belongs to the latest project technology stage, also denoted as set #3 in [22], [24], the key figures of which are listed in Table I. The structure is designed for experimental dc characterization. The drawn emitter area is equal to 0.2×2.8 μm^2, the emitter width being among those typically selected for advanced circuit design [22]. The SH R_{TH} was experimentally found to be about 7000 K/W with an approach based on simple dc measurements [16], [23]. The cross-section of the DUT is schematically represented in Fig. 2. The structure is geometrically complex and characterized by a markedly 3-D heat flow.

TABLE I. KEY FIGURES OF THE DUT

BV_{CBO}	5.5 V
peak f_T @ V_{CB}=0 V	235 GHz
J_C @ peak f_T, V_{CB}=0 V	10 mA/μm^2
peak f_{MAX} @ V_{CB}=0 V	330 GHz
peak f_T @ V_{CB}=0.5 V	240 GHz
peak f_{MAX} @ V_{CB}=0.5 V	380 GHz

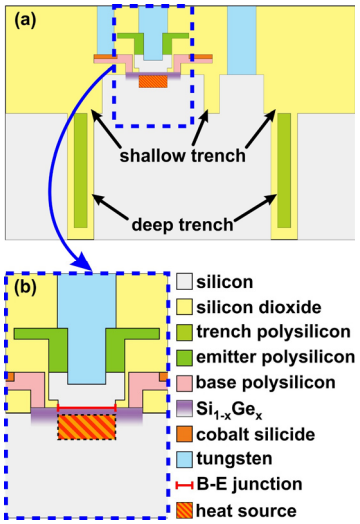

Fig. 2. (a) Sketch of the cross-section of the DUT and (b) magnification of the intrinsic transistor region. Evidenced are: the metallurgical base-emitter junction, the heat source (base-collector space-charge region), and all materials.

V. RESULTS AND DISCUSSION

A. 3-D Thermal Model of the DUT

Fig. 3 shows the 3-D hexahedral grid representing the DUT, as obtained by an *in-house* tool based on the FVM. The back-end-of-line architecture was accounted for. A smart mesh refinement strategy was exploited to ensure a highly-fine grid over the intrinsic transistor region, and a coarser one far from the heat source; slightly less than 5×10^6 bricks were used.

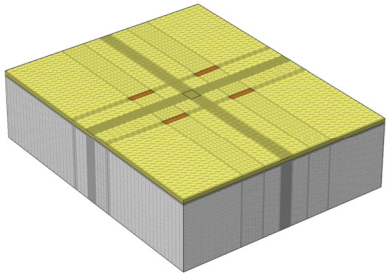

Fig. 3. 3-D hexahedral grid representing the DUT (the external pads for dc measurements are not represented).

Fig. 4 depicts the corresponding geometry. A preliminary analysis allowed demonstrating that the simplifications due to the adoption of the hexahedral grid only marginally impact the temperature field over the intrinsic transistor compared to the more accurate tetrahedral grid used in [16], [23].

The heat source was assumed to coincide with the base-collector space-charge region, where the power is dissipated [16], [23]. The substrate backside was held at 300 K, which can be practically made with a thermochuck; all other surfaces were considered adiabatic. As shown in Fig. 3, a horizontally large domain was built to prevent an unrealistic influence of the adiabatic edges on the device temperature field.

Typical values (at 300 K) were assigned to all material parameters (thermal conductivity, mass density, and specific heat), except for the silicon (Si) regions crossed by the heat in the intrinsic transistor, the thermal conductivity of which is markedly degraded due to the combined impact of (i) high doping and (ii) acoustic phonon scattering against the edges (lateral sides) of narrow layers like emitter tungsten contact, Si emitter, SiGe base, and Si volume surrounded by shallow trench [16], [23]. All material parameters are listed in Table II.

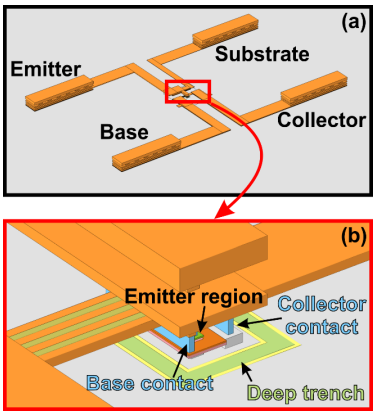

Fig. 4. (a) Geometry of the DUT (the pads are not represented) and (b) magnification of the intrinsic transistor region.

TABLE II. MATERIAL PARAMETERS OF THE DUT

Material	k [W/mK]	ρ [Kg/m^3]	c_p [J/KgK]
SiGe (base)	11	3229	605.7
Bulk Si	148	2330	711
Si (bottom collector)	80	2330	711
Si (top collector)	30	2330	711
Si (bottom emitter)	35	2330	711
Si (top emitter)	50	2330	711
Silicon dioxide (SiO_2)	1.4	2203	709
Trench polysilicon	20	2330	920
Emitter polysilicon	40	2330	920
Base polysilicon	30	2330	920
Tungsten (W)	177	19275	130
Copper (Cu)	390	8954	384
Cobalt silicide (CoSi)	9.6	5300	580
Bottom emitter W contact	148	19275	130
Top emitter W contact	161	19275	130
Heat source Si volume	30	2330	711

B. Structure Functions

The structure function of the DUT determined with the proposed algorithm is shown in Fig. 5. Despite the very high number of bricks composing the grid, the most relevant portion of the function, where the wave-front has not propagated yet in sub-regions very far away from the source (R<6000 K/W), was extracted in less than five minutes on a 3.6 GHz 10-Core Intel Core i9. About two hours were required for the whole calculation.

The structure function obtained with the proposed approach was compared with a structure function derived from the thermal response of the DUT by using a much more robust variant of the original Székely algorithm [2], [3] developed as follows. First, a very accurate (with a relative error of 10^{-8}) dynamic compact thermal model (DCTM) of the DUT in the Foster's I canonical form was extracted in about four hours with a multi-point moment matching technique equivalent to that implemented in FANTASTIC [25], [26], but directly operating on the port thermal response [27] (an inverse numerical deconvolution is instead used in [2], [3]). Such DCTM was first turned into a 44-order Foster's I canonical form by solving a generalized eigenvalue problem; the Foster's I form was then transformed into an equivalent Cauer's I canonical form by a tridiagonalization approach making use of a partial re-orthogonalization ensuring robustness [12]. From Fig. 5, it is inferred that the structure function derived with this DCTM-based strategy is fairly close to that extracted directly from the stiffness and mass matrices with the proposed algorithm, while being less accurate since the DCTM has a much lower order with respect to the discretized heat conduction problem.

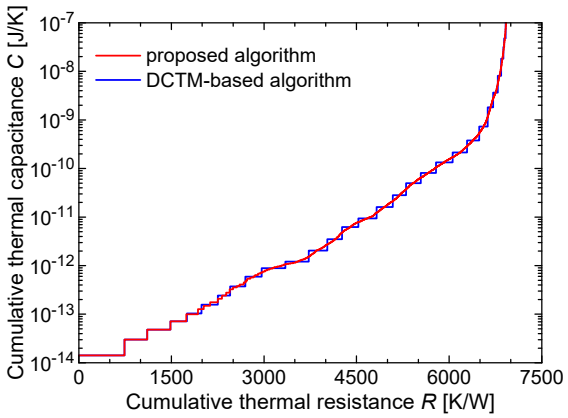

Fig. 5. Structure function (profile of the cumulative thermal capacitance C vs. cumulative thermal resistance R) extracted for the DUT with the algorithm proposed in this work (red line) and with a DCTM-based algorithm improving the original Székely's one (blue).

Another analysis was performed by extracting the structure function of a variant of the DUT where the deep trench was completely filled with silicon dioxide (SiO_2) instead of polysilicon (trench *core*) coated by CVD SiO_2 (Fig. 2). As can be seen in Fig. 6, (i) the structure function is not impacted by the different trench *core* until point **C**, at which a bifurcation takes place; (ii) the R_{TH} increases by about 400 K/W with respect to the original DUT since the lateral heat propagation is more hindered by the deep trench.

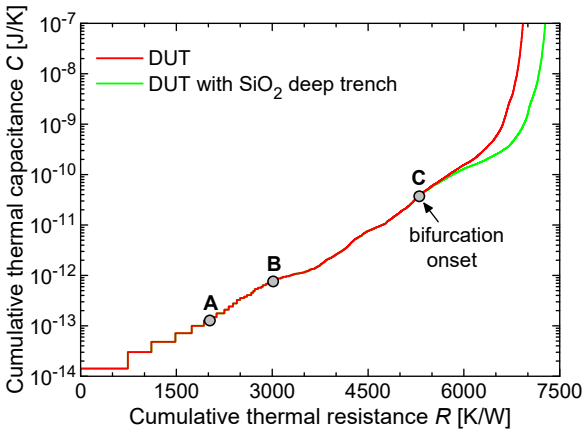

Fig. 6. Structure function determined for the DUT (red line) and for a DUT variant suffering from a poorly-conductive full-SiO_2 deep trench (green).

As mentioned earlier, the proposed algorithm allows identifying the specific thermal properties responsible for a given behavior of the structure function. As an example, it is possible to plot and analyze the spatial distributions of the weights of thermal resistivity used to compute the resistances of *RC* ladder network defining the structure function at points A, B, C indicated in Fig. 6. Such spatial distributions, shown over the cross-section of the DUT in Fig. 7, offer an exhaustive overview of the impact of the thermal conductivity of all sub-regions on the structure function. In particular, Fig. 7c clearly witnesses that the bifurcation point **C** occurs when the wave-front of the spatial distribution hits the edge of the deep trench *core*, the thermal conductivity of which was altered in the DUT variant.

This study suggests a potential, and relevant, application of the proposed approach. By inspecting the differences between (i) the structure function extracted from a 3-D thermal device model by our algorithm and (ii) the structure function derived from the experimental thermal response of the device by e.g., the commercial variant of the Székely algorithm or our more robust version of it introduced in Section V.A, it is possible to straightforwardly and quickly identify the physical reasons leading to such differences, even if they are associated to the thermal properties of a sub-region not located in the close proximity of the heat source. This information would allow calibrating the parameters of the thermal model and localizing defects or other technological problems. It is clear that in this case the experimental thermal response has to be measured under low-power conditions to prevent nonlinear thermal effects, as the 3-D thermal model is equipped with the thermal conductivity values at an assigned temperature.

Alternative approaches based on the comparison between the experimental thermal response (either in time or in frequency domain) and a numerical one computed by thermal solvers do not offer this possibility, as in this case finding the physical reasons for the differences between the curves is an intricate task.

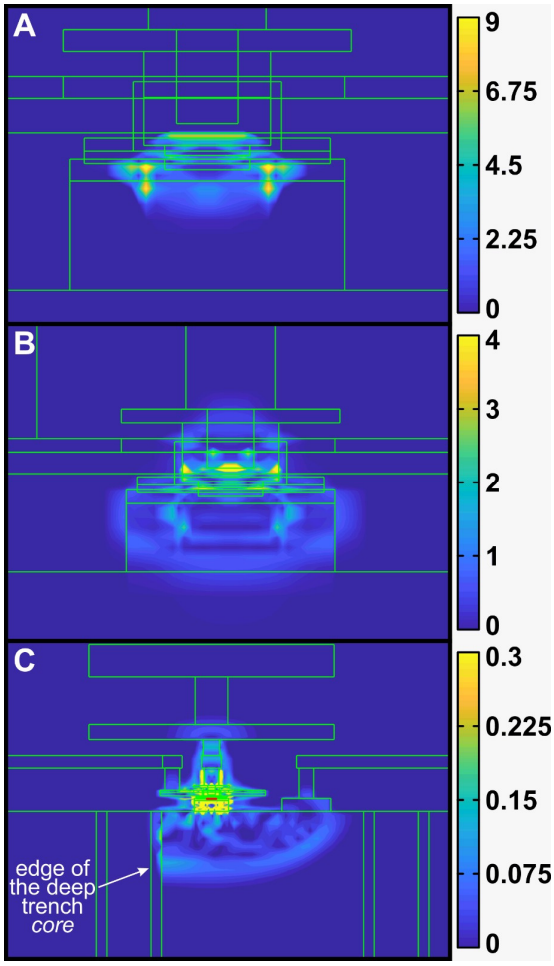

Fig. 7. Spatial distributions of the weights of thermal resistivity ($||\mathbf{j}||$ [$J^{1/2}K^{-1/2}s^{-1}m^{-2}$]) over the cross-section of the DUT at points **A**, **B**, **C** identified in Fig. 6.

VI. CONCLUSION

An algorithm has been presented for accurately determining the structure function of a 3-D heat conduction problem by means of the tridiagonalization of its discretized equation, performed in a relatively short time. In this approach, the partial conductances and capacitances in the structure function are evaluated in terms of weighted spatial averages of thermal resistivity and volumetric heat capacity, respectively. Hence, for the first time, the exact influence of all materials and geometric details on each part of the structure function can be assessed for a 3-D heat flow normally taking place in devices of practical relevance.

By comparing the structure function extracted from a thermal model of a device through the proposed algorithm with the structure function derived from the thermal response of the real device with other algorithms, it would be possible to calibrate the thermal properties of the model, as well as to identify physical differences (e.g., defects) between the device and the associated model. Consequently, our approach can be of particular interest for design engineers.

The algorithm has been successfully validated on a geometrically-complex SiGe:C HBT developed for high-frequency applications, but adversely affected by a markedly high thermal resistance.

ACKNOWLEDGMENTS

The funding for the Ph.D. activity of Ciro Scognamillo was generously donated by the Rinaldi family in the memory of Niccolò Rinaldi, a bright Professor and Researcher of the University of Naples Federico II, prematurely passed away in 2018. The authors want to express their gratitude to the anonymous reviewers for their constructive and insightful comments, which contributed to improve the readability and comprehensibility of the manuscript.

REFERENCES

[1] E. N. Protonotarios and O. Wing, "Theory of nonuniform RC lines Part I: Analytical properties and realizability conditions in the frequency domain," *IEEE Trans. Circuit Theory*, vol. 14, no. 1, pp. 2–12, Mar. 1967. doi: 10.1109/TCT.1967.1082650

[2] V. Székely and T. Van Bien, "Fine structure of heat flow path in semiconductor devices: A measurement and identification method," *Solid-State Electron.*, vol. 31, no. 9, pp. 1363–1368, Sep. 1988. doi: 10.1016/0038-1101(88)90099-8

[3] V. Székely, "A new evaluation method of thermal transient measurement results," *Microelectron. J.*, vol. 28, no. 3, pp. 277–292, Mar. 1997. doi: 10.1016/S0026-2692(96)00031-6

[4] V. Székely, "Identification of RC networks by deconvolution: Chances and limits," *IEEE Trans. Circuit Syst. I*, vol. 45, no. 3, pp. 244–258, Mar. 1998. doi: 10.1109/81.662698

[5] M. Salleras, M. Carmona, and S. Marco, "Issues in the use of thermal transients to achieve accurate time-constant spectrums and differential structure functions," *IEEE Trans. Adv. Packag.*, vol. 33, no. 4, pp. 918–923, Nov. 2010. doi: 10.1109/TADVP.2010.2049572

[6] M. Rencz and V. Székely, "Measuring partial thermal resistances in a heat-flow path," *IEEE Trans. Comp. Packag. Technol.*, vol. 25, no. 4, pp. 547–553, Dec. 2002. doi: 10.1109/TCAPT.2002.808003

[7] M. Rencz, A. Poppe, E. Kollár, S. Ress, and V. Székely, "Increasing the accuracy of structure function based thermal material parameter measurements," *IEEE Trans. Comp. Packag. Technol.*, vol. 28, no. 1, pp. 51–57, Mar. 2005. doi: 10.1109/TCAPT.2004.843204

[8] L. Codecasa, "Canonical forms of one-port passive distributed thermal networks," *IEEE Trans. Comp. Packag. Technol.*, vol. 28, no. 1, pp. 5–13, Mar. 2005. doi: 10.1109/TCAPT.2004.843182

[9] R. Bornoff, T. Mérelle, J. Sari, A. Di Bucchianico, and G. Farkas, "Quantified insights into LED variability," in *Proc. International Workshop on Thermal Investigations of ICs and Systems (THERMINIC)*, 2018. doi: 10.1109/THERMINIC.2018.8593315

[10] L. Codecasa, V. d'Alessandro, and D. D'Amore, "Algorithm for establishing the dependence of structure functions on spatial distributions of thermal properties," in *Proc. International Workshop on Thermal Investigations of ICs and Systems (THERMINIC)*, 2019. doi: 10.1109/THERMINIC.2019.8923748

[11] L. Codecasa, "Structure function representation of multidirectional heat-flows," *IEEE Trans. Comp. Packag. Technol.*, vol. 30, no. 4, pp. 643–652, Dec. 2007. doi: 10.1109/TCAPT.2007.906315

[12] G. H. Golub and C. F. Van Loan, *Matrix Computation*, The Johns Hopkins University Press, 1996.

[13] P. Chevalier *et al.*, "Towards THz SiGe HBTs," in *Proc. IEEE Bipolar/BiCMOS Circuits and Technology Meeting (BCTM)*, 2011, pp. 57–65. doi: 10.1109/BCTM.2011.6082749

[14] P. Chevalier *et al.*, "Si/SiGe:C and InP/GaAsSb heterojunction bipolar transistors for THz applications," *Proceedings of the IEEE*, vol. 105, no. 6, pp. 1035–1050, Jun. 2017. doi: 10.1109/JPROC.2017.2669087

[15] M. Schröter *et al.*, "SiGe HBT technology: Future trends and TCAD-based roadmap," *Proceedings of the IEEE*, vol. 105, no. 6, pp. 1068–1086, Jun. 2017. doi: 10.1109/JPROC.2015.2500024

[16] N. Rinaldi and M. Schröter, Eds., *Silicon-Germanium Heterojunction Bipolar Transistors for mm-Wave Systems Technology, Modeling and Circuit Applications*. Delft, The Netherlands: River Publishers, 2018. doi: 10.13052/rp-9788793519602

[17] A. El Rafei, A. Saleh, R. Sommet, J. M. Nébus, and R. Quéré, "Experimental characterization and modeling of the thermal behavior of SiGe HBTs," *IEEE Trans. Electron Devices*, vol. 59, no. 7, pp. 1921–1927, Jul. 2012. doi: 10.1109/TED.2012.2196765

[18] A. K. Sahoo, S. Frégonèse, M. Weiß, N. Malbert, and T. Zimmer, "A scalable electrothermal model for transient self-heating effects in trench-isolated SiGe HBTs," *IEEE Trans. Electron Devices*, vol. 59, no. 10, pp. 2619–2625, Oct. 2012. doi: 10.1109/TED.2012.2209651

[19] I. Hasnaoui, A. Pottrain, D. Gloria, P. Chevalier, V. Avramovic, and C. Gaquière, "Self-heating characterization of SiGe:C HBTs by extracting thermal impedances," *IEEE Electron Device Lett.*, vol. 33, no. 12, pp. 1762–1764, Dec. 2012. doi: 10.1109/LED.2012.2220752

[20] R. D'Esposito, S. Balanethiram, J.-L. Battaglia, S. Frégonèse, and T. Zimmer, "Thermal penetration depth analysis and impact of the BEOL metals on the thermal impedance of SiGe HBTs," *IEEE Electron Device Lett.*, vol. 38, no. 10, pp. 1457–1460, Oct. 2017. doi: 10.1109/LED.2017.2743043

[21] V. d'Alessandro, I. Marano, S. Russo, D. Céli, A. Chantre, P. Chevalier, F. Pourchon, and N. Rinaldi, "Impact of layout and technology parameters on the thermal resistance of SiGe:C HBTs," in *Proc. IEEE Bipolar/BiCMOS Circuits and Technol. Meeting (BCTM)*, Oct. 2010, pp. 137–140. doi: 10.1109/BIPOL.2010.5667912

[22] V. d'Alessandro, G. Sasso, N. Rinaldi, and K. Aufinger, "Influence of scaling and emitter layout on the thermal behavior of toward-THz SiGe:C HBTs," *IEEE Trans. Electron Devices*, vol. 61, no. 10, pp. 3386–3394, Oct. 2014. doi: 10.1109/TED.2014.2349792

[23] V. d'Alessandro, A. Magnani, L. Codecasa, N. Rinaldi, and K. Aufinger, "Advanced thermal simulation of SiGe:C HBTs including back-end-of-line," *Microelectronics Reliab.*, vol. 67, pp. 38–45, Dec. 2016. doi: 10.1016/j.microrel.2016.06.005

[24] V. d'Alessandro, G. Sasso, N. Rinaldi, and K. Aufinger, "Experimental DC extraction of the base resistance of bipolar transistors: Application to SiGe:C HBTs," *IEEE Trans. Electron Devices*, vol. 63, no. 7, pp. 2691–2699, Jul. 2016. doi: 10.1109/TED.2016.2565203

[25] L. Codecasa, V. d'Alessandro, A. Magnani, N. Rinaldi, and P. J. Zampardi, "FAst Novel Thermal Analysis Simulation Tool for Integrated Circuits (FANTASTIC)," in *Proc. International Workshop on Thermal Investigations of ICs and Systems (THERMINIC)*, 2014. doi: 10.1109/THERMINIC.2014.6972507

[26] A. Magnani, V. d'Alessandro, L. Codecasa, P. J. Zampardi, B. Moser, and N. Rinaldi, "Analysis of the influence of layout and technology parameters on the thermal impedance of GaAs HBT/BiFET using a highly efficient tool," in *Proc. IEEE Compound Semiconductor Integrated Circuit Symposium (CSICS)*, 2014. doi: 10.1109/CSICS.2014.6978543

[27] L. Codecasa, D. D'Amore, and P. Maffezzoni, "Multipoint moment matching reduction from port responses of dynamic thermal networks," *IEEE Trans. Comp. Packag. Techn.*, vol. 28, no. 4, pp. 605–614, Dec. 2005. doi: 10.1109/TCAPT.2005.859741